Fabrication of NiO Nanowall Electrodes for High Performance Lithium Ion Battery

Binni Varghese,[†,‡,§] M. V. Reddy,[†,‡] Zhu Yanwu,[‡,§] Chang Sheh Lit,[‡] Teo Choon Hoong,[‡,§] G. V. Subba Rao,[‡] B. V. R. Chowdari,[‡] Andrew Thye Shen Wee,[‡,§] Chwee Teck Lim,[§,||,⊥] and Chorng-Haur Sow*[,‡,§]

Department of Physics, Faculty of Science, National University of Singapore, 2 Science Drive 3, Singapore 117542, Singapore, National University of Singapore Nanoscience and Nanotechnology Initiative Singapore, (NUSNNI), 2 Science Drive 3, Singapore 117542, Singapore, Division of Bioengineering, National University of Singapore, Blk E3A, 9 Engineering Drive 1, Singapore 117576, Singapore, and Department of Mechanical Engineering, National University of Singapore, 9 Engineering Drive 1, Singapore 117576, Singapore

Received December 10, 2007. Revised Manuscript Received March 17, 2008

We report the fabrication of vertically aligned NiO nanowalls on nickel foils using a plasma assisted oxidation method. Electrochemical properties of as-synthesized NiO nanowalls were evaluated by galvanostatic cycling and cyclic voltammetery. The results show a capacity of ~638 (mA h)/g (at 1.25C rate), with excellent capacity retention of up to 85 cycles, when cycled in the range, 0.005−3.0 V vs Li. The superior electrochemical performance of NiO nanowalls in comparison to the previously reported results on nanosized NiO particles can be attributed to its large surface area and shorter diffusion length for mass and charge transport. A possible reaction mechanism is discussed. We also report that electron field emission studies show that the verticllay aligned NiO nanowalls are efficient field emitters with a turn-on field of 7.4 V/μm and a maximum current density of ~160 μA/cm^2 can be achieved.

Introduction

Nanostructured materials have attracted great interest in both fundamental as well as applied research areas due to their outstanding physical and chemical properties. Construction of well-ordered, specifically oriented ensembles of nanostructures and realization of their potential applications have resulted in intensive research for the past few years. Recently, fabrication of vertically aligned interconnected two-dimensional (2D) nanostructures, so-called nanowalls of various materials including carbon,[1] zinc oxide (ZnO),[2] and cobalt oxide (Co_3O_4),[3] have been reported. Nanowalls with attributes such as high surface to volume ratio and open edge geometry represent an ideal 2D structure and will be useful as battery materials, field emitters, and so forth.

Nickel oxide (NiO) is an antiferromagnetic semiconductor with a wide band gap of ~3.6 eV.[4] NiO is an extensively studied material due to its potential use as a magnetic thin film,[5] active layer for gas sensors,[6] electrochromic material,[7] battery material,[8] and so forth. Nanostructures of NiO with unique size and shape may exhibit superior functionality or may open new possibilities due to the large surface fraction and confinement effect inherent to the reduced dimensional materials. Synthesis of nanostructures of NiO in various forms including nanowires,[9] nanorods,[10] nanosheets,[11] and nanorolls[12] has been reported in recent years. However, to the best of our knowledge, vertically oriented 2D nanostructures of NiO have not been reported yet.

In this paper, we report a simple yet efficient method to create vertically aligned, single crystalline NiO nanowalls on a nickel foil. The potential use of such fabricated NiO nanowall film in Li-ion battery and electron field emission applications was investigated in detail. An attribute of this synthesis approach is the feasibility of straightforward electrochemical and field emission studies of the as-made nanostructures without further postgrowth assembly and manipulation. Remarkably, NiO nanowalls showed excellent capacity retention and high rate capability on cycling. It was able to achieve a discharge capacity of ~638 (mA h)/g (1.25C rate) at the end of 85 cycles when cycled between 3.0 V and 5 mV (vs Li). The field emission measurements showed that NiO nanowalls are efficient emitters with low turn-on field and reasonably high current density.

* Corresponding author: Phone: (65) 65162957. Fax: (65) 67776126. E-mail: physowch@nus.edu.sg.
[†] These two authors contributed equally to this work.
[‡] Department of Physics, National University of Singapore.
[§] National University of Singapore Nanoscience and Nanotechnology Initiative.
[||] Division of Bioengineering, National University of Singapore.
[⊥] Department of Mechanical Engineering, National University of Singapore.

(1) Wu, Y.; Yang, B.; Zong, B.; Sun, H.; Shen, Z.; Feng, Y. P. *J. Mater. Chem.* **2004**, *14*, 469.
(2) Ng, H. T.; Li, J.; Smith, M. K.; Nguyen, P.; Cassell, A.; Han, J.; Meyyappan, M. *Science* **2003**, *300*, 1249.
(3) Yu, T.; Zhu, Y.; Xu, X.; Shen, Z.; Chen, P.; Lim, C. T.; Thong, J. T. L.; Sow, C. H. *Adv. Mater.* **2005**, *17*, 1595.
(4) Adler, D.; Feinleib, J. J. *Phys. Rev. B* **1970**, *2*, 3112.
(5) Fujii, E.; Tomozawa, A.; Torii, H.; Takayama, R. *Jpn. J. Appl. Phys.* **1996**, *35*, L328.
(6) Hotovy, I.; Huran, J.; Spiess, L.; Hascik, S.; Rehacek, V. *Sens. Actuators, B* **1999**, *57*, 147.
(7) Porqueras, I.; Bertran, E. *Thin Solid Films* **2001**, *398−399*, 41.
(8) Poizot, P.; Laruelle, S.; Grugeon, S.; Dupont, L.; Tarascon, J.-M. *Nature* **2000**, *407*, 496.
(9) Lin, Y.; Xie, T.; Cheng, B. C.; Geng, B.; Zhang, L. *Chem. Phys. Lett.* **2003**, *380*, 521.
(10) Wang, W.; Liu, Y.; Xu, C.; Zheng, C.; Wang, G. *Chem. Phys. Lett.* **2002**, *362*, 119.
(11) Liang, Z.-H.; Zhu, Y.-J.; Hu, X.-L. *J. Phys. Chem. B* **2004**, *108*, 3488.
(12) Liu, X.; Qiu, G.; Wang, Z.; Li, X. *Nanotechnology* **2005**, *16*, 1400.

10.1021/cm703512k CCC: $40.75
Published on Web 05/03/2008

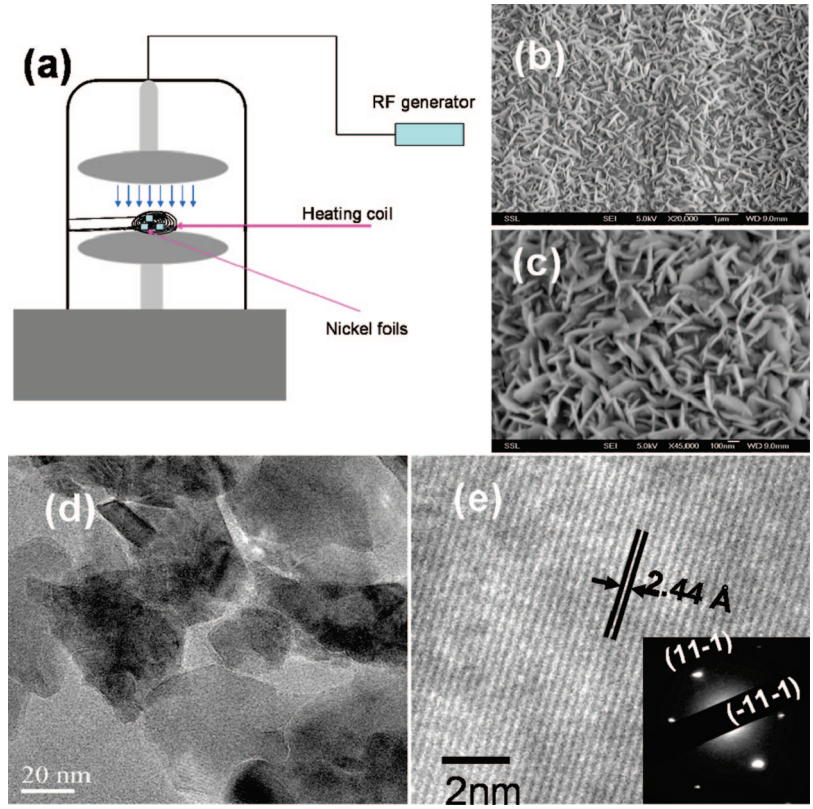

Figure 1. (a) Schematic of the experimental setup used for the growth of NiO nanowalls and (b and c) low and high magnification SEM images of the NiO nanowalls grown on nickel foil viewed at 20° from the substrate normal. (d) Low magnification TEM image (scale bar = 20 nm) and (e) high resolution TEM image (scale bar = 2 nm) of the NiO nanowalls. Inset of (e) shows SAED pattern of the NiO nanowall (zone axis along $[0\bar{1}\bar{1}]$).

Experimental Section

Preparation of NiO Nanowalls. Nickel foils with assembled NiO nanowalls were synthesized directly by the plasma assisted oxidation method. Nickel foils (Alfa Aesar Inc.) with thickness of 0.1 mm were used both as supporting substrate as well as source of metal precursor for the growth of NiO nanowalls. The schematic of the experimental setup used for the growth of NiO nanowalls is illustrated in Figure 1a. The nickel foils were mounted on a heating core cable, located amidst a capacitively coupled plasma (CCP) source in a vacuum chamber. The CCP is driven by a radio frequency (RF) plasma generator operating at 13.56 MHz. After reaching the base pressure of $\sim 1 \times 10^{-6}$ Torr, the current through the heating coil was gradually increased to attain the required growth temperature as monitored using a thermocouple. Oxygen gas was leaked at a constant rate, and the pressure inside the chamber was controlled and maintained at a constant value during growth. The growth of NiO nanowalls was then initiated by turning on the RF power thereby creating an oxygen plasma in the chamber. After growth the samples were cooled down naturally to room temperature. Experiments to determine the optimal growth of nanowalls were carried out over a temperature range of 450−800 °C, RF power of 0−250 W, processing pressure 200−2000 mTorr, and oxygen flow rate of 10−30 sccm. The most favorable growth conditions were found to be at a substrate temperature of 600 (±20) °C, RF power of 200 W, oxygen flow rate of 30 sccm, and processing pressure of 1500 mTorr. After growth, the shiny metallic surface of the nickel foil turned greenish yellow, indicating the presence of NiO nanostructures.

Characterization Techniques. The morphology and structure of the as-synthesized nanostructures were characterized using field emission scanning electron microscopy (FESEM, JEOL JSM-6700F), transmission electron microscopy (TEM, JEOL, JEM-2010F, 200 kV), X-ray diffraction (X'PERT MPD, Cu Kα (1.542 Å) radiation, while unit cell parameter was determined by using TOPAS-R Software), and Raman spectroscopy (Renishaw system 2000, excitation 532 nm). X-ray photoelectron spectroscopy (XPS, ESCA MK II; using Mg Kα source) was used to determine oxidation state of the Ni in NiO nanowalls.

For electrochemical measurements, NiO nanowall was used as working electrode, and Ni metal substrate was used as current collector. Li metal foil (0.59 mm thick; Kyokuto Metal Co. Ltd., Japan) was used as the counter (anode) and reference electrodes, and a 1 M solution of $LiPF_6$ in ethylene carbonate (EC) and diethyl carbonate (DEC) (1:1 by volume; Merck) was used as the electrolyte and polypropylene foil (celgard) as the separator. Coin-type test cells (size 2016) were fabricated in an argon-filled glovebox (MBraun, Germany). We note that no conducting carbon or binder were used for the fabrication of the above thin film electrode. The geometrical area of the electrode is 2.0 cm^2. The total thickness of the NiO film and nanowall was estimated from the SEM cross sectional image of the sectioned sample. Using these geometrical parameters and the density of the NiO (6.7 g/cm^2) the active mass of the material is calculated to be ~0.335 mg. The cells were aged overnight before measurement. The galvanostatic discharge−charge cycling and cyclic voltammetry were carried out at room temperature by using Macpile II system (Biologic, France) and multichannel battery tester (model SCN, Bitrode, U.S.A.), respectively. Other details of cell fabrication and instrumentation have been described previously.[13,14]

(13) Reddy, M. V.; Ting, Y.; Sow, C. H.; Shen, Z. X.; Lim, C. T.; Subba Rao, G. V.; Chowdari, B. V. R. *Adv. Funct. Mater.* **2007**, *17*, 2792.
(14) Reddy, M. V.; Madhavi, S.; Subba Rao, G. V.; Chowdari, B. V. R. *J. Power Sources* **2006**, *162*, 1312.

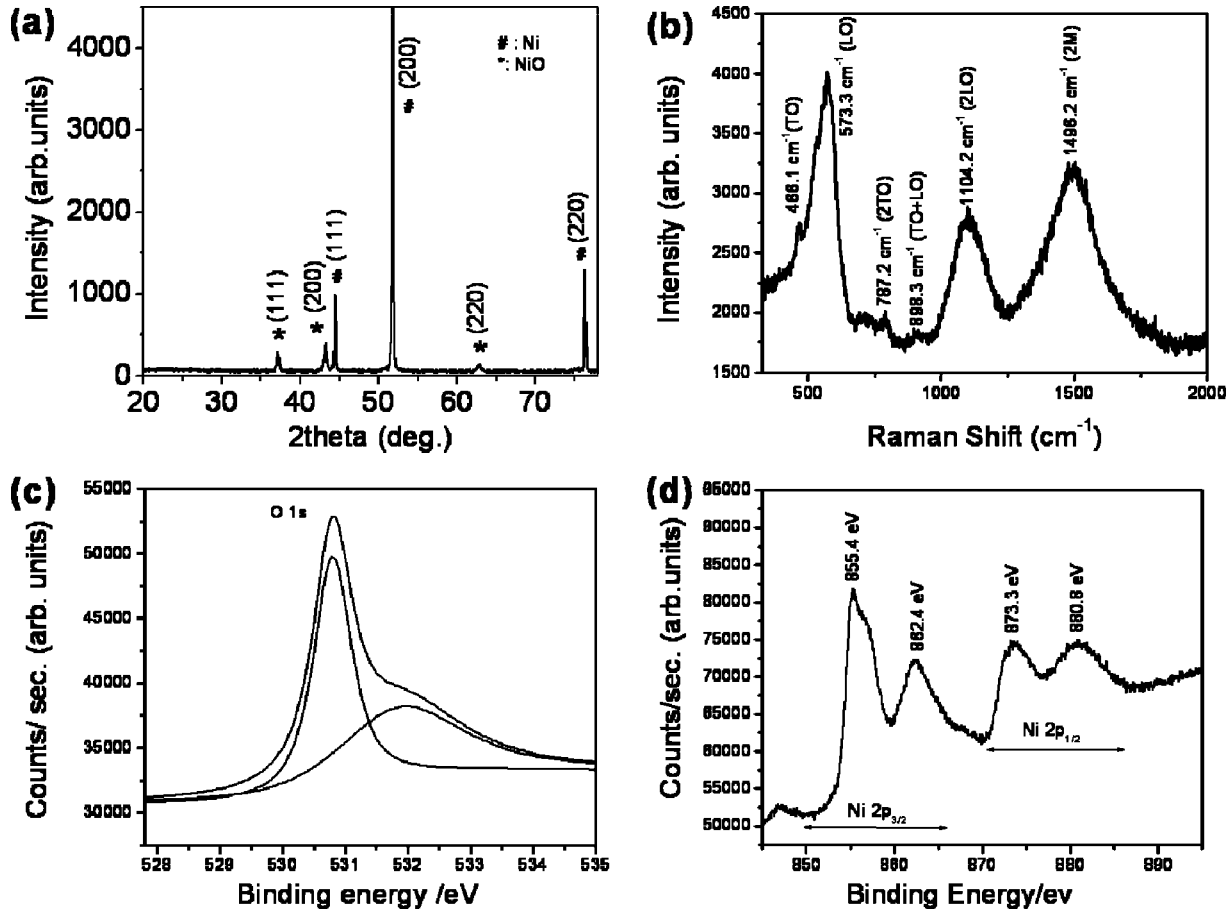

Figure 2. (a) XRD pattern of the nickel foil with NiO nanowalls (Cu Kα radiation). (b) Micro-Raman spectrum of the NiO nanowalls. (c and d) XPS spectra of O 1s and Ni 2p core levels of nanowalls, respectively.

For field emission studies the Ni foil with NiO nanowalls was glued onto a copper cathode using conducting double sided adhesive tape. A glass slide coated with indium tin oxide (ITO) was used as the counter electrode. The separation between the electrodes was kept at 100 μm by using a polymer film with a circular aperture of area 22 mm^2 as a spacer. The voltage between the electrodes is gradually increased in steps of 10 V, and the corresponding current was measured using a Keithley 237 high voltage source measurement unit (SMU). The field emission measurements were carried out at room temperature and at $\sim 1 \times 10^{-6}$ torr. Details of the experimental setup employed for the field emission measurement have been reported elsewhere.[15]

Results and Discussion

Characterization of NiO Nanowalls. Figure 1b,c shows typical SEM images of the nickel foil after 2 h of growth. The entire surface is uniformly covered with a thin film of free-standing 2D nanostructures (nanowalls). The as-synthesized NiO nanowalls are over 100 nm in height, and the wall thickness is typically less than 40 nm. The nanowalls are vertically aligned to the plane of the substrate and are interconnected to each other resulting in the formation of extended network structures.

For the TEM analysis, some of the nanowalls were transferred to a commercially available copper TEM grid with carbon film by gently sliding it over an ethanol-wet as-grown nanowall film. These samples were dried in air prior to the TEM analysis. Figure 1d shows a low magnification TEM image of the nanowalls showing its unique geometrical shape. The HR-TEM image of the nanowalls in Figure 1e reveals lattice fringes with interplanar spacing of 2.44 Å corresponding to the (111) lattice planes of the rock salt NiO structure ($d = 2.41$ Å). The inset of Figure 1e shows the SAED pattern of the nanowalls.

Figure 2a shows the XRD pattern of the nickel foil with nickel oxide nanowalls. The diffraction peaks observed at angles of 37.4°, 43.5°, and 62.9° can be indexed to the (111), (200), and (220) planes of the cubic NiO phase, respectively. The calculated lattice parameter of NiO nanowalls is $a =$ 4.183 Å, which is in good agreement with the value of (4.172 Å) reported literature (JCDF card no. 78-0423). The XRD pattern also includes diffraction peaks corresponding to the Ni substrate. Notably, no other suboxide phases of nickel were observed in the XRD pattern. The micro-Raman spectrum of the nanowalls was recorded using 532 nm excitation wavelength at room temperature (Figure 2b). The bands observed at 466.1 and 573.3 cm^{-1} are ascribed to the transverse optical (TO) and longitudinal optical (LO) phonon modes of NiO, respectively, and are in good agreement with the reported values of the bulk NiO single crystals.[16] The peaks at 787.2, 898.3, and 1104.2 cm^{-1} correspond to the

(15) Zhu, Y. W.; Yu, T.; Cheong, C. F.; Xu, X. J.; Lim, C. T.; Tan, V. B. C.; Thong, J. T. L.; Sow, C. H. *Nanotechnology* **2005**, *16*, 88.

(16) Dietz, R. E.; Parisot, G. I.; Meixner, A. E. *Phys. Rev. B* **1971**, *4*, 2302.

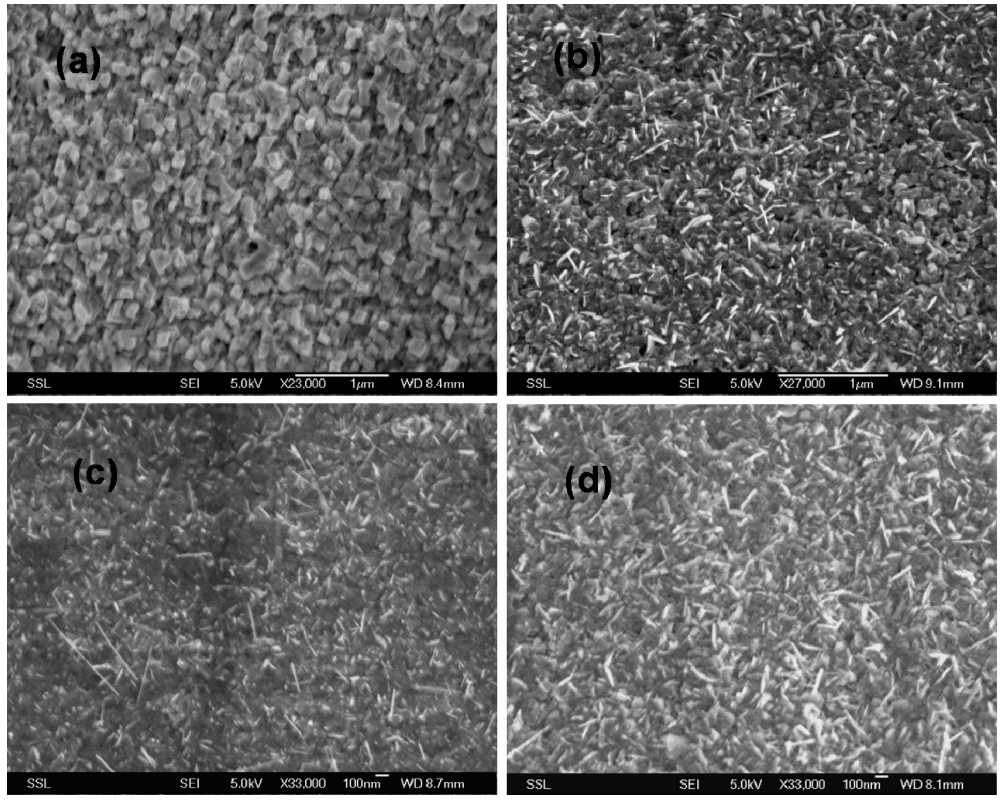

Figure 3. (a and b) SEM images of the nickel foil after heat treatment at 600 ± 20 °C in oxygen atmosphere without plasma and with a RF plasma of power 100 W, respectively. (c and d) SEM images of nickel foil treated in a oxygen plasma of power 200 W at temperature 450 ± 20 °C and 500 ± 20 °C, respectively.

2TO, TO+LO, and 2LO combination phonon modes, respectively. The strong peak observed at 1496.2 cm^{-1} corresponds to the two magnon (2M) excitation in NiO. Figure 2c,d shows XPS spectra of the nanowalls for the O 1s and Ni 2p core levels, respectively. The O 1s spectrum, after deconvolution into two peaks, consists of a main peak at 530.5 eV with a shoulder at ∼1 eV higher binding energy. The Ni 2p spectra comprise two regions representing the Ni $2p_{3/2}$ (850−865 eV) and Ni $2p_{1/2}$ (870−885 eV) spin−orbit levels. The Ni $2p_{3/2}$ region consists of a main peak at 855.4 eV with a shoulder peak (∼1 eV above the main peak) and a satellite peak (∼7 eV above the main peak); similar features are observed for the $2p_{1/2}$ region. The binding energies of the main and satellite peaks in the O 1s and Ni 2p core levels are consistent with the previous report on NiO.[17]

In the absence of the plasma, no nanowall structures were observed on the heated foil surface within the range of temperatures studied (see Figure 3a). At relatively low plasma power condition (say 100 W) 1D nanoflake looking structures were observed on the foil surface (Figure 3b). However, the density of the nanoflakes was low. Above 225 W of plasma power only the formation of NiO film results. In addition, the growth temperature has a critical role in the formation of NiO nanowalls. At ∼450 (±20) °C and at a plasma power of 200 W, 1D nanoflakes were formed on the foil (Figure 3c). At ∼ 500 (±20) °C with 200 W plasma power a mixture of nanoflakes and nanowalls was formed, although the latter is predominant (Figure 3d). At higher temperatures (>650 °C) only the thin film of NiO was formed.

A cross-sectional view of a sectioned Ni foil after the nanowall growth showed a NiO nanowall/NiO film/Ni multilayer structure, which suggests a diffusion controlled mechanism for the nanowall growth. At the early stage of the growth, adsorbed oxygen molecules from the gaseous state react with the heated Ni foil surface leading to the formation of a NiO film. This is followed by the epitaxial growth of NiO nanowalls which is controlled by the diffusion of Ni atoms through the existing NiO film. At lower temperature and plasma power conditions, the diffusion rate of the constituent atoms at the heated foil surface is relatively slow and so is the reaction kinetics of formation of NiO. At these conditions, 1D nanoflake growth is favored instead of 2D nanowalls. On the other hand at the optimal temperature and plasma power the diffusion rate of the constituent atoms is high resulting in a high rate of formation of NiO. This leads to a rapid growth and results in the formation of 2D nanowalls. This argument is consistent with our previous report on the synthesis of cobalt oxide nanostructures with various morphologies by varying the reactivity and diffusion rate of oxidizing species on a heated metal foil.[18]

Electrochemical Properties of NiO Nanowalls. The electrochemical properties of NiO nanowalls for Li-ion battery applications were evaluated using galvanostatic

(17) Wertheim, G. K.; Hüfner, S. *Phys. Rev. Lett.* **1972**, *28*, 1028.

(18) Varghese, B.; Teo, C. H.; Yanwu, Z.; Reddy, M. V.; Chowdari, B. V. R.; Wee, A. T. S.; Vincent, T. B. C.; Lim, C. T.; Sow, C. H. *Adv. Funct. Mater.* **2007**, *17*, 1932.

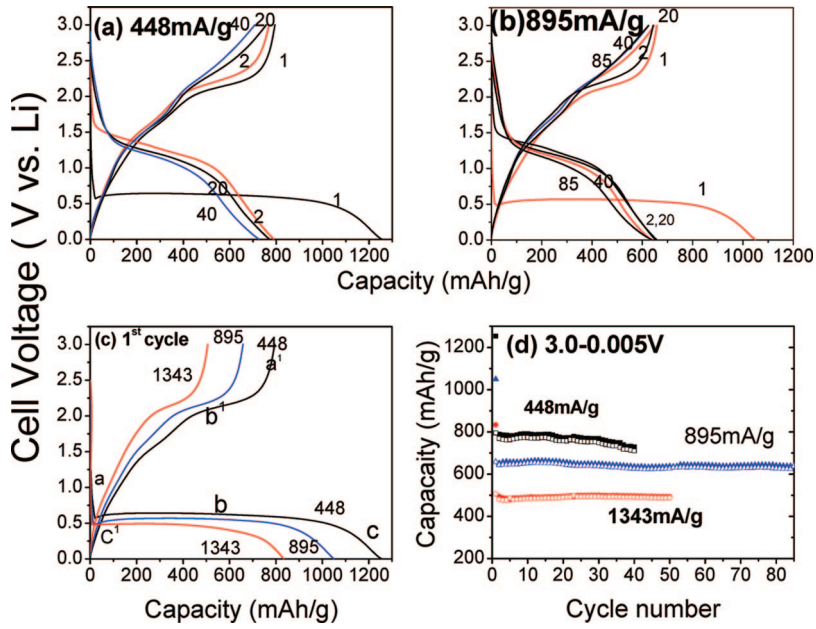

Figure 4. (a, b, and c) Galvanostatic cycling plots (voltage vs capacity) of NiO nanowalls. Current density and cycle number are indicated. (d) Plots of capacity vs cycle number. Cycled between 3.0−0.005 V vs Li, at room temperature.

discharge−charge cycling and cyclic voltammetry. Discharge−charge cycling was carried out in the potential window of 0.005−3.0 V versus Li. The current densities were measured at 448 mA/g (0.62C rate), 895 mA/g (1.25C rate), and 1343mA/g (1.87C rate) up to 40 (or 85) cycles. The voltage versus capacity profiles at current densities of 448 and 895 mA/g are shown in Figure 4a,b, respectively. For clarity, the first discharge−charge cycles with different current densities are shown in Figure 4c. The long-term cycling plots at current density 1343 mA/g are given in the Supporting Information (see Figure S1a). The open circuit voltage (OCV) of the fabricated aged (overnight) cells was ∼2.8 V. As shown in Figure 4a,c, during the first discharge, the voltage decreased steeply to ∼0.6 V where a plateau region (region b) sets in and continues until a capacity of 1050 (mA h)/g is reached. This corresponds to a consumption of 2.92 mol of Li per mol of NiO. Another slope was observed at ∼0.30 V, with a total first discharge capacity of 1253 (±20) (mA h)/g, corresponding to a consumption of 3.49 mol of Li per mol of NiO. The first charge profile of NiO nanowalls shows a strong polarization of ∼1.3 V (Figure 4a) followed by a voltage plateau at ∼2.2 V (region b′). The first charge capacity is 794 (mA h)/g (2.21 mol of Li). During the second discharge−charge cycle, voltage plateaus appear at ∼1.25 and ∼2.2 V, respectively. The irreversible capacity loss (ICL) during first discharge and charge cycle is about 459 (mA h)/g (current density, 448 mA/g). At higher current densities (895 and 1343 mA/g), the shapes of discharge−charge curves are similar to that at 448 mA/g (Figure 4b,c). However, during the first discharge cycle, the plateaus (region b, Figure 4c) are shifted to lower potential at higher current densities due to kinetic effects of the material. The first discharge−charge capacities were 1050 and 833 (±20) (mA h)/g and 685 and 506 (±20) (mA h)/g for 895 and 1343 mA/g, respectively. The corresponding ICL values at 895 and 1343 mA/g are 392 and 327 (mA h)/g, respectively, and these values are smaller than that of 448 mA/g. In general, ICL during first discharge and charge cycle arises becasuse of incomplete decomposition of solid electrolyte interface (SEI) and Li_2O[8,19–28] and other factors such as intrinsic nature of the material and kinetic limitations (due to current density).[13,14,23,25,27,28]

The capacity versus cycle number plots at current densities of 448, 895, and 1343 mA/g are shown in Figure 4d. The reversible capacity at the end of the 20th cycle varies from 757, 646, and 490 (±20) (mA h)/g, which correspond to respectively 2.10, 1.80, and 1.36 (±0.05) mol of Li per mol of NiO. It is also clear from Figure 4a,b,d that the Coulombic efficiency is >98% at higher current densities in the range 5−80 cycles. A previous report on the cycling performance of nanosized particles of NiO[8] showed a discharge capacities around 600 and 300 (mA h)/g at the end of the 2nd and 40th cycles respectively, cycled between 0.01 V and 3 V, at a rate of 0.2C. The observed capacity fades to about 50% between 2−40 cycles. We also observed high capacity fading in bulk NiO composite electrodes (see Supporting Information, Figure S1b). In the present study, NiO nanowalls exhibiting only 7% capacity fade between 2 to 40 cycles at a current density of 448 mA/g (0.62C rate). Moreover, at a

(19) Grugeon, S.; Laruelle, S.; Herrera-Urbina, R.; Dupont, L.; Poizot, P.; Tarascon, J. M. *J. Electrochem. Soc.* **2001**, *148*, A285.
(20) Deebart, A. A.; Dupont, L.; Poizot, P.; Leriche, J.-B.; Tarascon, J.-M. *J. Electrochem. Soc.* **2001**, *148*, A1266.
(21) Poizot, P.; Laruelle, S.; Grugeon, S.; Tarascon, J.-M. *J. Electrochem. Soc.* **2002**, *149*, A1212.
(22) Obrovac, M. N.; Dunlap, R. A.; Sanderson, R. J.; Dahn, J. R. *J. Electrochem. Soc.* **2001**, *148*, A576.
(23) Leroux, F.; Goward, G. R.; Power, W. P.; Nazar, L. F. *Electrochem. Solid-State Lett.* **1998**, *1*, 255.
(24) Balaya, P.; Li, H.; Kienle, L.; Maier, J. *Adv. Funct. Mater.* **2003**, *13*, 621.
(25) Taberna, P. L.; Mitra, S.; Poizot, P.; Simon, P.; Tarascon, J.-M. *Nat. Mater.* **2006**, *5*, 567.
(26) Sharma, Y.; Sharma, N.; Subba Rao, G. V.; Chowdari, B. V. R. *Adv. Funct. Mater.* **2007**, *17*, 2855.
(27) Reddy, M. V.; Pecquenard, B.; Vinatier, P.; Levasseur, A. *Electrochem. Commun.* **2007**, *9*, 409.
(28) Huang, X. H.; Tu, J. P.; Zhang, B.; Zhang, C. Q.; Li, Y.; Yuan, Y. F.; Wu, H. M. *J. Power Sources* **2006**, *161*, 541.

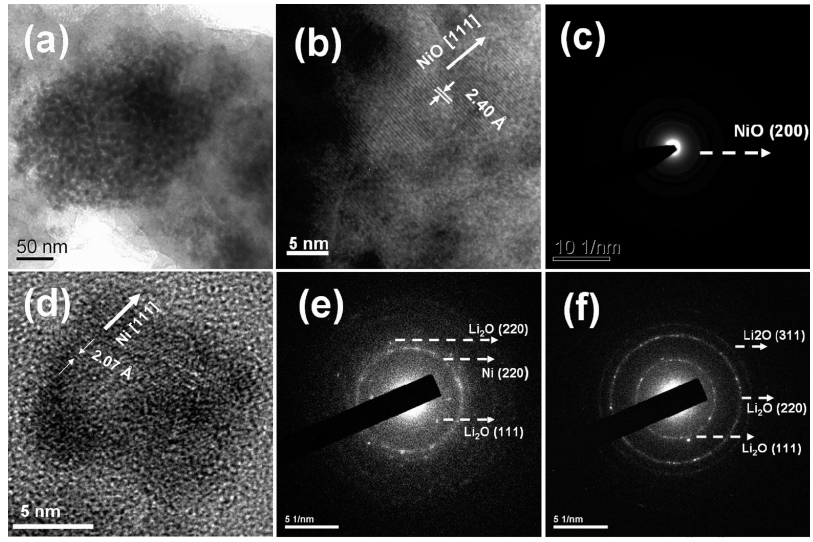

Figure 5. (a and b) High resolution TEM images and (c) selected area electron diffraction (SAED) pattern of NiO electrodes in the charged state (3.0 V) (after 40 cycles). (d−f) HRTEM image and SAED patterns of NiO electrodes in the discharged state (0.005 V) (after 40 cycles).

current density of 857 mA/g (1.25C rate), a capacity of 638 (±20) (mA h)/g with negligible capacity fading was demonstrated even after long-term cycling (3% capacity fading between 2 and 85 cycles). We note that the obtained capacity contribution from bare Ni-foil was <1 (mA h)/g (figures are shown in Supporting Information, Figure 2) and are negligible compared to the capacity values obtained from Ni foil with NiO nanowalls.

The ex situ XRD patterns of cycled electrodes in their charged or discharged state are shown in Supporting Information, Figure S3, and SEM images of the electrode in the charged state (after 40 cycles) are shown in Supporting Information, Figure S4. The result shows that the initial NiO nanowall structure (shown in Figure 1b,c) has transformed to amorphous/nanosized particles during cycling. Similar structure destruction and morphology variations are well-documented in literature.[8,14,26] Ex situ TEM studies of cycled electrodes in charged and discharged states are shown in Figure 5. The TEM images clearly show the particle size ranges from 5 to 8 (±2) nm (Figure 5a) with characteristic interplanar spacing of the host NiO compound (Figure 5b). The SAED pattern of the electrode (in the charged state, to 3.0 V) shows diffuse spots and diffuse rings indicative of an amorphous phase with nanocrystalline regions (Figure 5c) of NiO. Similar variations of particle size, metal and Li_2O formation during discharge, and metal to metal oxide formation during charge cycling were previously reported on nanosized CoO.[8] The HRTEM and SAED patterns of cycled electrode in the discharged state (0.005 V) showed the expected Ni and Li_2O phases (see Figure 5d−f and Supporting Information, Figure S5).

The first-discharge profiles of the NiO nanowalls are qualitatively similar to the results obtained by Tarascon et al.[8,21] However, the capacity values are relatively higher than the earlier studies. The reaction mechanism is similar to that proposed by Tarascon et al.[8,21] $NiO + 2Li^+ + 2e^- \rightarrow Ni^0 + Li_2O$ (discharge) + polymeric layer formation/electrolyte reduction, and $Ni^0 + Li_2O \leftrightarrow Ni^{2+}O + 2.0Li^+ + 2e^-$(charge). Theoretically, during discharge the process must consume 2.0 mol of Li per mol of NiO. Our observed experimental values are 3.49 mol of Li, and the extra 1.49 mol of Li can be partially attributed to the formation of SEI and the polymeric gel-type layer on the metal nanoparticles due to the decomposition of the solvent in the electrolyte.[8,13,19–21,26] During the first charge reaction, the decomposition of Li_2O is aided by the nano-Ni^0 resulting in the formation of NiO, giving a capacity depending on current density (Figure 4c).

Cyclic voltammogram (CV) studies give complementary data to the galvanostatic cycling. The CVs of NiO nanowalls are shown in Figure 6a. The CV was recorded on the cells with NiO nanowalls in the potential window between 3.0−0.005 V, at a scan rate of 0.058 mV s^{-1}. The first cathodic scan (reaction with Li) started from the OCV, ∼2.8 V. A smooth curve up to ∼0.7 V with a peak at ∼0.57 V is observed corresponding to the initial reduction of $Ni^{2+}O$ to metallic Ni, with Li_2O and SEI formation. During anodic scan (Li-removal from the host), a peak at ∼2.1 V corresponding to the NiO formation and decomposition of SEI and Li_2O[19–21] is observed. In the second cathode/anodic scan, a set of broad peaks at 1.25 and 2.2 V are seen, respectively. The sixth cycle CV shows well-defined cathodic and anodic peaks that bear good resemblance to that of the sixth cycle differential capacity versus potential plots as shown in Figure 6b−d. With increasing scan rate, the expected increase in peak currents and a shift in both the cathodic and the anodic voltages were observed[20,27] (see Supporting Information, Figure S6). The differential capacity versus voltage plot for the 6th and 40th cycle, shown in Figure 6b−d, indicates that the average discharge voltage is ∼1.2 V and the charge-voltage is 2.2 V. These voltage values are in agreement with nanoparticle NiO and Ni-NiO composites reported in the literature.[28,29]

The improved capacity and good stability up to 85 cycles of the NiO nanowalls can be attributed to the following

(29) (a) Yuan, L.; Guo, Z. P.; Konstantinov, K.; Munroe, P.; Liu, H. K. *Electrochem. Solid-State Lett.* **2006**, *9*, A524. (b) Needham, S. A.; Wang, G. X.; Liu, H. K. *J. Power Sources* **2006**, *159*, 254.

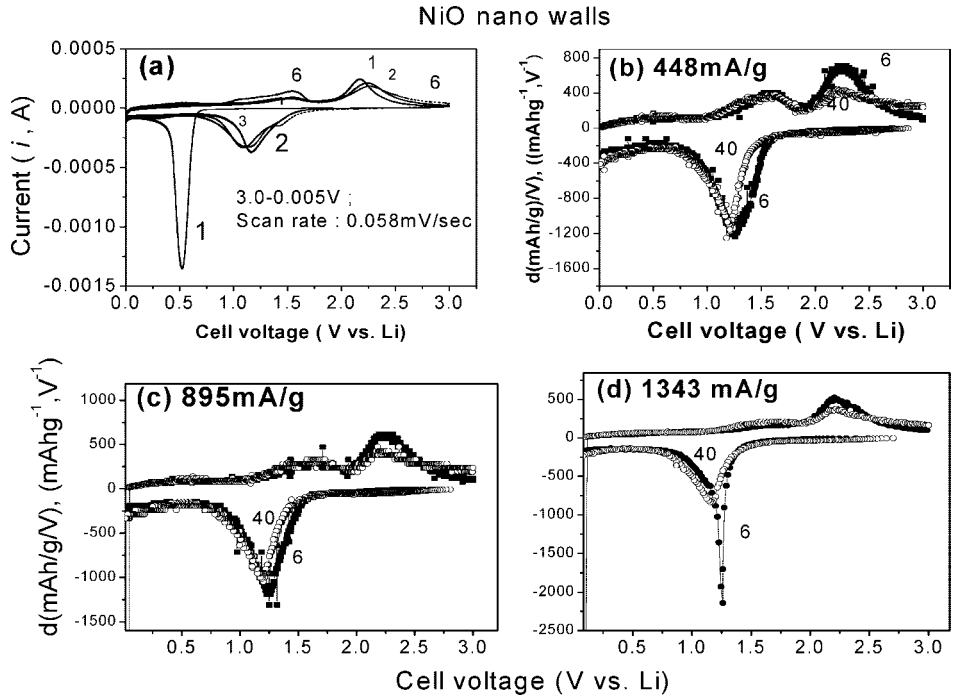

Figure 6. (a) Cyclic voltammograms (*i* vs *V* plots) of NiO nanowalls; scan rate 0.058 mV/s. (b, c, d) Differential capacity vs cell voltage plots extracted from Figure 3 and Supporting Information, Figure S2a. Potential between 3.0 and 0.005 V.

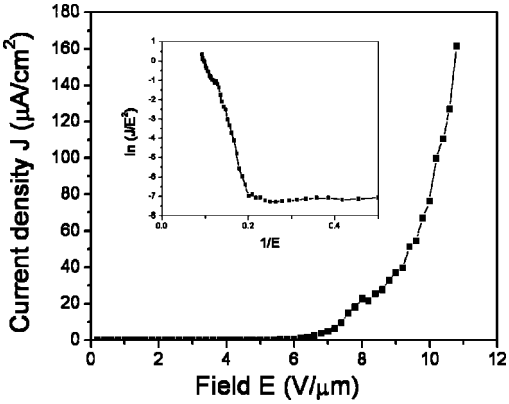

Figure 7. Field emission current density versus applied electric field ($J-E$) plot of NiO nanowalls. The inset shows the corresponding FN plot.

factors. First, the effective electrode/electrolyte contact area is enhanced due to the vertically aligned configuration as well as the unique NiO nanowall morphology.[30,31] Second, as a result of the small wall thickness, mass and charge find shorter diffusion lengths for ionic and electronic transport, respectively. Finally, NiO nanowalls being grown directly on Ni substrates provide a good electrical contact between the electrode and the active material.

Field Emission Characteristics of NiO Nanowalls. The field emission performance of the NiO nanowalls was examined using a parallel plate electrode configuration at a pressure of $\sim 10^{-6}$ Torr at room temperature. Figure 7 shows the emission current density (J) from the nanowalls as a function of applied field (E). The turn-on field of the nanowall emitters is found to be 7.4 V/μm at a current density of 10 μA/cm^2. The current density at a maximum applied field of 11 V/μm (limited by our setup) is better than 160 μA/cm^2. According to the Fowler−Nordheim (FN) theory,[32] the field emission current density is related to the applied field according to

$$J = \frac{\alpha A}{\phi}(\beta E_{\text{avg}})^2 \exp\left(-\frac{B\phi^{3/2}}{\beta E_{\text{avg}}}\right) \quad (1)$$

where J is the emission current density (A/cm^2), E_{avg} is the average electric field (V/μm), ϕ is the work function of the emitters (eV), α is the area factor, and β is the field enhancement factor. A and B are constants. The enhancement factor β can be deduced from the slope (S) of the $1/E$ versus $\ln(J/E^2)$ plot (FN plot). The work function of the NiO nanowalls was estimated by ultraviolet photoelectron spectroscopy (UPS) measurements. The UPS measurement was performed using 59.9 eV photons with a sample bias of −5 eV (see Supporting Information, Figure S7). Using the energy cutoff of the photoelectrons obtained from the UPS spectra, the work function was estimated to be 4.1 eV. Notably this value is slightly lower than the reported bulk value for NiO (4.3 eV). By using the estimated work function of the nanowalls the enhancement factor (β) is calculated to be ~700. These results are comparable with other known nanostructures.[33] It is worth mentioning that the turn-on field and current density of the NiO nanowalls are better than the previous report on the field emission properties of NiO nanorods.[34] The efficient field emission from the nanowalls is attributable to its nanometer scale wall thickness and open edge geometry. In addition, the reduced work function of the nanowalls facilitates the electron emission process.

(30) Maier, J. *Nat. Mater.* **1999**, *5*, 805.
(31) Arico, A. S.; Bruce, P. G.; Scrosati, B.; Tarascon, J.-M.; Schalkwijk, W. V. *Nat. Mater.* **2005**, *4*, 366.
(32) Fowler, R. H.; Nordheim, L. W. *Proc. R. Soc. London, Ser. A* **1928**, *119*, 173.
(33) Xu, N. S.; Huq, S. E. *Mater. Sci. Eng.* **2005**, *R48*, 47.
(34) Zhang, Z.; Zhao, Y.; Zhu, M. *Appl. Phys. Lett.* **2006**, *88*, 033101.

Conclusions

In summary, a simple method to fabricate well aligned NiO nanowall film directly on nickel foil is presented. The as-prepared nanowalls were characterized using SEM, XRD, micro-Raman, XPS, and TEM techniques. The multifunctionality of the NiO nanowall film was demonstrated by investigating its electrochemical and field emission properties. Electrochemical properties of NiO nanowalls show excellent capacity retention on cycling and high rate performance, which makes NiO nanowalls a promising anode material for high power Li-ion batteries. In particular the rate capability and Coulombic efficiency of vertically aligned NiO nanowalls are better than the previously reported works on NiO nanoparticles. The field emission studies of the NiO nanowalls show that they are competent candidates for many field emission based device applications. The turn on voltage and the maximum attainable current density of the nanowalls are comparable with other known nanostructures.

Supporting Information Available: Galvanostatic cycling plots of NiO nanowalls and NiO bulk material, SEM photograph of commercial NiO, galvanostatic cycling plots of Ni foil, XRD patterns of cycled electrodes, SEM image of cycled electrode, low magnification TEM of NiO cycled electrode, CV curves, and UPS spectra of NiO nanowalls. This material is available free of charge via the Internet at http://pubs.acs.org.

CM703512K